Evaporation-Combustion Affected by In-Cylinder, Reciprocating Porous Regenerator

Chan-Woo Park

Massoud Kaviany
e-mail: kaviany@umich.edu

Department of Mechanical Engineering,
The University of Michigan,
Ann Arbor, MI 48109-2125

An existing in-cylinder thermal regeneration concept for Diesel engines is examined for the roles of the porous insert motion and the fuel injection strategies on the fuel evaporation and combustion and on the engine efficiency. While the heated air emanating from the insert enhances fuel evaporation resulting in a superadiabatic combustion process (thus increasing thermal efficiency), the corresponding increase in the thermal NO_x is undesirable. A two-gas-zone and a single-step reaction model are used with a Lagrangian droplet tracking model that allows for filtration by the insert. A thermal efficiency of 53 percent is predicted, compared to 43 percent of the conventional Diesel engines. The optimal regenerative cooling stroke occurs close to the peak flame temperature, thus increasing the superadiabatic flame temperature and the peak pressure, while decreasing the expansion stroke pressure and the pressure drop through the insert. During the regenerative heating stroke, the heated air enhances the droplet evaporation, resulting in a more uniform, premixed combustion and a higher peak pressure, thus a larger mechanical work. [DOI: 10.1115/1.1418368]

Keywords: Engines, Heat Transfer, Heat Recovery, Porous Media, Regenerators

1 Introduction

A regenerative Diesel engine using an in-cylinder reciprocating, porous regenerator as shown in Fig. 1 has the potential to improve fuel-air mixing and combustion [1–3]. The porous insert is attached to a rod and moves in the cylinder, synchronized, but out of phase with the piston. During the regenerative heating stroke, the regenerator remains just beneath the cylinder head for most of the period and moves down to the piston (as it approaches the TDC position). During the regenerative cooling stroke, the regenerator moves up and remains in the original position until the next regenerative heating stroke. Following the combustion and expansion, the products of combustion (exhaust gases) retain an appreciable sensible heat. During the regenerative cooling stroke, the hot exhaust gas flows through the insert and stores part of this sensible heat by surface-convection heat transfer in the porous insert (with large surface area). While the external thermal regeneration, examined extensively, would reduce the volumetric efficiency (due to external heating of the intake air, before arrival in the cylinder), the internal thermal regeneration with the in-cylinder porous insert does not affect the volumetric efficiency significantly. This is because the intaked air arrives in the cylinder and is then heated by passing through the hot insert, after the intake valve is closed. The superadiabatic flame temperature (due to the thermal regeneration of the combustion heat) [4] and the fuel droplet-regenerator interaction, enhances the fuel evaporation. A uniform fuel vapor distribution is possible due to the deflection of fuel droplets by the air flow emanating from the porous regenerator and this can improve combustion. Here the fuel droplet-regenerator interaction is examined, i.e., aiming at an improved regenerative engine performance.

2 Analysis

The geometric parameters and variables of the regenerative Diesel engine with a side valve position are shown Fig. 2. The two gas zones of the top and bottom chambers are connected by the permeable regenerator. The regenerator is divided into N_r small volumes and each volume consists of the gas and solid phases. Considering the complexities and the transient behavior before a quasi-steady solution is reached, for the sake of computation economy, a lumped, multi gas zone model and a simplified chemical kinetic model are used. The multi-zone-first-order analysis of the regenerative engine performance is given below, followed by the analysis of the injected fuel droplet.

2.1 Heat Transfer. A multi-zone gas model and a one-dimensional model for the solid phases are used for the analysis of the regenerative Diesel engine. The mechanisms of the heat transfer considered include the surface-convection, conduction and surface/volume radiation. The prescribed temperature of the cooling water is used for the analysis of the conduction heat transfer through the cylinder walls. One-dimensional energy conservation equations with both uniform and nonuniform grids are used for solid phases of the regenerator, the piston, the cylinder head, and cylinder block. Since the fuel is injected into the top gas zone and the fuel vapor does not escape to the bottom gas zone under the conditions considered, it is assumed that the combustion occurs only in top gas zone. The heat release rate in the top gas zone is determined using a single-step, second-order combustion model and the empirical relation of the ignition delay. The species concentrations are calculated to determine the heat release rate and the NO_x production rate.

The gas is assumed to be an ideal gas

$$\rho_f = \frac{M_f}{V_f} = \frac{p_f}{\frac{R_g}{M_a} T_f}. \tag{1}$$

For the top gas zone above the regenerator, the energy conservation equation is given as

$$Q_{u,\mathrm{inj}} - (Q_{u,r})_{N_r} + \langle Q_{ku,t-ch}\rangle_{D_B} + \langle Q_{ku,t-cb}\rangle_{D_B} + \langle Q_{ku,t-r}\rangle_{D_B} = -\frac{d}{dt}(M_{f,t} c_{p,f} T_{f,t}) + \dot{S}_t, \tag{2}$$

where $Q_{u,\mathrm{inj}}$ is the heat transfer due to the fuel injection and $(Q_{u,r})_{N_r}$ is the heat transfer due to the gas influx through the

Contributed by the Heat Transfer Division for publication in the JOURNAL OF HEAT TRANSFER. Manuscript received by the Heat Transfer Division May 2, 2000; revision received May 20, 2001. Associate Editor: J. G. Georgiadis.

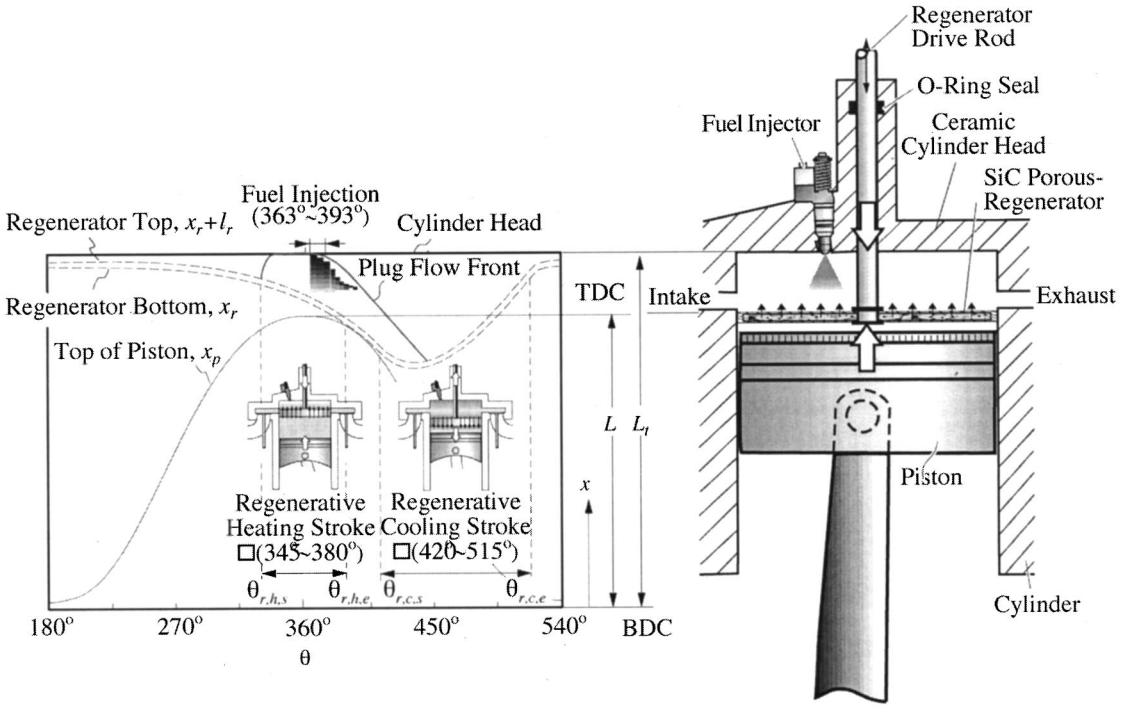

Fig. 1 Sequence of motion of the regenerator and piston and physical rendering of fuel injection and air blowing during the regenerative heating stroke

regenerator. $\langle Q_{ku,t-ch \text{ or } cb \text{ or } r}\rangle_{D_B}$ are the surface-convection heat transfer between the top fluid and surfaces (of the cylinder head, the cylinder block and the regenerator). The energy conversion in the top gas zone $\dot{S}_t$ is due to combustion (occurs only in the top gas zone) $\dot{S}_{r,c}$, gas expansion cooling/compression heating $\dot{S}_{m,p,t}$, fuel evaporation $\dot{S}_{F,lg}$, and radiation $(\dot{S}_{e,\epsilon}+\dot{S}_{e,\alpha})_t$, i.e.,

$$\dot{S}_t=\dot{S}_{r,c}+\dot{S}_{m,p,t}+\dot{S}_{F,lg}+(\dot{S}_{e,\epsilon}+\dot{S}_{e,\alpha})_t. \tag{3}$$

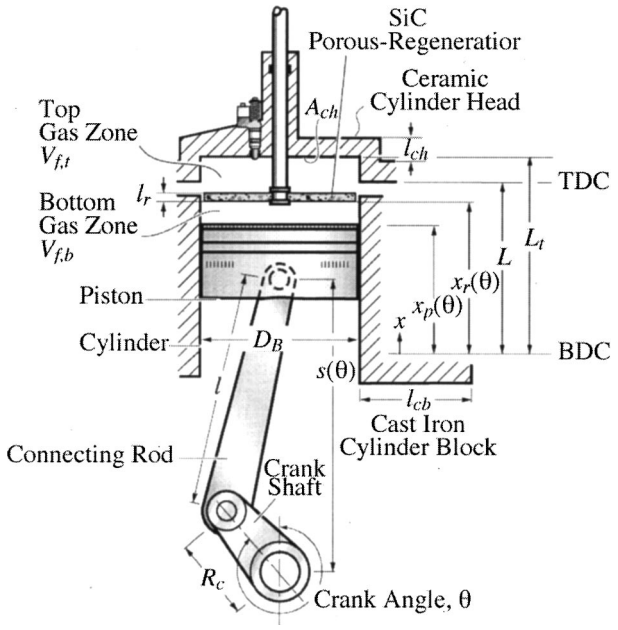

Fig. 2 Geometric parameters and variables of the regenerative Diesel engine

A more detailed description for each term of the energy conservation Eg. (2) is given in the Appendix.

Similarly, for the bottom gas zone the energy conservation equation is given as

$$-Q_{u,\text{int}}+Q_{u,\text{exh}}+(Q_{u,r})_0+\langle Q_{ku,b-cb}\rangle_{D_B}+\langle Q_{ku,b-p}\rangle_{D_B}$$
$$+\langle Q_{ku,b-r}\rangle_{D_B}=-\frac{d}{dt}(M_{f,b}c_{p,f}T_{f,b})+\dot{S}_b, \tag{4}$$

where $Q_{u,\text{int}}$, $Q_{u,\text{exh}}$ and $(Q_{u,r})_0$ are the convection heat transfer due to the intake, the exhaust, and the gas influx through the regenerator. Considering a combustion efficiency of 98 percent in top gas zone, under the conditions given in Table 1, it is assumed that the fuel is consumed completely in the top gas zone, and, therefore, no combustion occurs in the bottom gas zone. The energy conversion in the bottom gas zone $\dot{S}_b$ is due to gas expansion cooling/compression heating only, i.e.,

$$\dot{S}_b=\dot{S}_{m,p,b}=V_{f,b}\frac{dp_{f,b}}{dt}. \tag{5}$$

A more detailed description, for each term of the energy conservation Eq. (4), is given in the Appendix.

The porous regenerator is divided into N_r small volumes with uniform thickness $\Delta l_{r,i}$ and local thermal nonequilibrium is assumed between the gas and the solid phases. The energy equation for each volume of the solid phase is given by

$$-(Q_{k,r})_{(i-1)-i}+(Q_{k,r})_{i-(i+1)}+\langle Q_{ku,f-r}\rangle_i-Q_{d,i}$$
$$=-\rho_r\Delta l_{r,i}(1-\epsilon_r)A_r c_{p,r}\frac{dT_{r,i}}{dt}, \quad i=1,2,\ldots,N_r, \tag{6}$$

where $(Q_{k,r})_{i-(i+1)}$, $\langle Q_{ku,f-r}\rangle_i$ and $Q_{d,i}$ are the heat transfer due to the conduction in the solid phase, the surface-convection and the evaporation of the fuel droplet, respectively. Note that it is assumed that the heat transfer due to the evaporation of the fuel

Table 1 Operational characteristics of the engine

Parameter	Magnitude	Parameter	Magnitude
operating conditions:		intake valve:	
V_d	$1,718\text{cm}^3$	$N_{v,i}$	1
V_c	245.4cm^3	$C_{D,i}$	0.75
r_c	$6 \sim 16.5$	$D_{v,i}$	0.044 m
N	1,600 rpm	$L_{v,i}$	$0.25D_{v,i}$
$(A/F)_a$	30	$\theta_{v,s,i}$	0°
$(A/F)_s$	15.5	$\theta_{v,e,i}$	224°
Φ	0.52	$p_{n,i}$	357 kPa
$T_{f,w}$	380 K	$T_{n,i}$	329 K
fuel injection		exhaust valve:	
$M_{F,o}$	0.216 g	$N_{v,e}$	1
N_d	50	$C_{D,e}$	0.7
D_{SM}	100 μ m	$D_{v,e}$	0.042 m
$u_{d,o}$	100 m/s	$L_{v,e}$	$0.25D_{v,e}$
$T_{d,o}$	500 K	$\theta_{v,s,e}$	474°
$\theta_{F,s}$	363°	$\theta_{v,e,e}$	720°
$\theta_{F,e}$	393°	$p_{n,e}$	251 kPa
regenerator schedule:		$T_{n,e}$	800 K
$\theta_{r,c,s}$	345°		
$\theta_{r,c,e}$	380°		
$\theta_{r,h,s}$	420°		
$\theta_{r,h,e}$	515°		

droplet occurs in the solid phase of the regenerator. More detailed description, for each term of the energy conservation Eq. (6), is given in the Appendix.

The energy equation for the gas phase in the porous regenerator is given as

$$-(Q_{u,r})_{i-1}+(Q_{u,r})_i-\langle Q_{ku,f-r}\rangle_i = -\frac{d}{dt}(M_{f,r}c_{p,f}T_{f,r})_i+\dot{S}_{r,i}, \quad i=1,2,\ldots,N_r, \quad (7)$$

where

$$\dot{S}_{r,i}=(\dot{S}_{m,p})_{r,i}=V_{f,r,i}\frac{dp_{f,r,i}}{dt},$$

and the convection heat transfer $(Q_{u,r})_i$ and the surface-convection heat transfer $\langle Q_{ku,f-r}\rangle_i$ are given in Appendix in detail. The energy conservation equations at the top and bottom surfaces of the regenerator are also given in the Appendix.

The cylinder wall of the regenerative Diesel engine consists of the ceramic cylinder head and the cast iron cylinder block. The cylinder head and the cylinder block are assumed to be ideally insulated from each other. The cylinder head made of ceramic is used as a thermal barrier to reduce the heat loss. The cylinder head is divided into $N_{ch}-1$ small volumes with a uniform thickness $\Delta l_{ch,i}=l_{ch,1}/(N_{ch}-1)$ and a large volume with thickness $\Delta l_{ch,N_{ch}}=l_{ch,2}=l_{ch}-l_{ch,1}$. Then the energy equation for the solid phase is written as

$$(Q|_{A,ch})_i=-\rho_{ch}\Delta l_{ch,i}A_{k,ch}c_{p,ch}\frac{dT_{ch,i}}{dt}, \quad i=1,2,\ldots,N_{ch}, \quad (8)$$

where $(Q|_{A,ch})_i$ is heat transfer due to the conduction and is given in Appendix in detail. The energy conservation equations at the surface inside the cylinder head are also given in the Appendix.

The energy conservation equations for the cylinder block and the piston are given similarly.

The intake mass flow rate using the valve curtain area $A_{v,i}$, is given as

$$\dot{M}_{f,\text{int}}=N_{v,i}C_{D,i}A_{v,i}\frac{p_o}{\left(\frac{R_g}{M_g}T_o\right)^{1/2}}f_{A,f}(p_T,p_o), \quad (9)$$

where

$$A_{v,i}=\pi D_{v,i}L_{v,i}f_{A,v}(\theta,\theta_{v,s,i},\theta_{v,e,i}).$$

Similarly, the exhaust mass flow rate $\dot{M}_{f,exh}$ is determined. Here $f_{A,f}(p_T,p_o)$ is obtained from a one-dimensional isentropic flow analysis for the compressible flow through a flow restriction [5].

The mass flow through the porous regenerator is determined by the Darcy law [6] and is given by

$$(\dot{M}_{f,r})_i=A_r\rho_{f,r}\frac{K_r}{\mu_f}\frac{(p_{f,r,i}-p_{f,r,i+1})}{\Delta l_{r,i}},$$

$$K_r=\frac{\epsilon_r^3D_p^2}{180(1-\epsilon_r)^2}, \quad i=0,1,\ldots,N_r, \quad (10)$$

where

$$\rho_{f,r}=\begin{cases}\rho_{f,r,i} & \text{for } (\dot{M}_{f,r})_i\geq 0 \quad \text{(the bottom to the top gas zone)}\\ \rho_{f,r,i+1} & \text{for } (\dot{M}_{f,r})_i<0\end{cases},$$

and $\rho_{f,r,0}=\rho_{f,b}$, and $\rho_{f,r,N_r+1}=\rho_{f,t}$.

The combustion reaction $\dot{M}_{r,F}$ in the top gas zone, using the single-step reaction model [7], is given by

$$\dot{M}_{r,F}=\rho_{f,t}a_r\rho_F^{a_F}\rho_O^{a_O}\exp^{\Delta E_a/R_gT_{f,t}}, \quad (11)$$

where a_r is the pre-exponential factor and ΔE_a is the activation energy (kJ/kmole-K). The ignition delay is determined using the empirical correlation of the Diesel engine and ranges 2~3 crank angles under the conditions considered [5].

2.2 Droplet Evaporation. The transient fuel evaporation and the fuel droplet fate are determined using a Lagrangian, droplet tracking model along with a porous-surface filtration submodel for the droplet-regenerator interaction. These allow for the analysis of the fuel droplet evaporation, accumulation and combustion. After the fuel is injected, the fuel spray is assumed to be divided into N_d homogeneous droplet parcels. It is assumed that each parcel has n_d droplet particles with the same properties (e.g., droplet diameter, speed and temperature) and does not interfere with other droplet parcels. The Sauter mean diameter D_{SM} is used as the initial droplet diameter [8].

The instantaneous location of a droplet is given by

$$\frac{d}{dt}\mathbf{x}_d=\mathbf{u}_d. \quad (12)$$

The instantaneous velocity is determined by the momentum equation of a droplet as

$$\frac{d}{dt}(M\mathbf{u})_d=\sum \mathbf{F}=\mathbf{F}_d+\mathbf{F}_{\Delta T}+\ldots, \quad (13)$$

and neglecting the thermophoresis force $\mathbf{F}_{\Delta T}$ and other forces, the momentum equation is given by

$$M_d\frac{d\mathbf{u}_d}{dt}=-\frac{\pi}{8}D_d^2\rho_{f,t}C_D|\mathbf{u}_d-\langle\mathbf{u}_f\rangle_{p,t}|(\mathbf{u}_d-\langle\mathbf{u}_f\rangle_{p,t}), \quad (14)$$

where

$$C_D=\begin{cases}27\,\text{Re}_D^{-0.84} & \text{for } \text{Re}_D<80\\ 0.271\,\text{Re}_D^{0.217} & \text{for } 80<\text{Re}_D<10^4,\end{cases}$$

where $\mathrm{Re}_D=\rho_{f,t}D_d|\mathbf{u}_d-\langle\mathbf{u}_f\rangle_{p,t}|/\mu_f$.

In order to account for the deflection of the fuel droplets by the air flow emanating from the regenerator, the gas flow in the top gas zone is assumed to be the plug flow and the gas velocity is given as

$$\langle u_f\rangle_{p,t}=\frac{(\dot{M}_{f,r})_{N_r}}{A_r\rho_{f,r}}+\frac{dx_r}{dt}. \tag{15}$$

From the uniform temperature model for the fuel droplet heat and mass transfer (only the composition of the bulk liquid remains at the injected condition while the surface composition varies as required by the local conditions. The temperature of the surface and the bulk liquid are the same and are known at each instant), the mass conservation for a droplet is given by [9]

$$\frac{dM_d}{dt}=-\dot{M}_d. \tag{16}$$

The corrected evaporation rate $\dot{M}_d$ for the convective ambient is expressed

$$\frac{\dot{M}_d}{\dot{M}_d(\mathrm{Re}_D=0)}=1+f(\mathrm{Re}_D,\mathrm{Sc}), \tag{17}$$

where the evaporation rate $\dot{M}_d(\mathrm{Re}_D=0)$ in the quiescent ambient is given in the Appendix and

$$f(\mathrm{Re}_D,\mathrm{Sc})=\frac{0.278\,\mathrm{Re}_D^{1/2}\mathrm{Sc}^{1/3}}{[1+1.232/\mathrm{Re}_D\mathrm{Sc}^{4/3}]^{1/2}}. \tag{18}$$

The droplet energy conservation equation based on the uniform temperature model is

$$+\frac{\mathrm{Nu}_{D,1}k_f}{D_d}A_d(T_d-T_{f,t})+\frac{\mathrm{Nu}_{D,2}k_f}{D_d}A_d(T_d-T_{r,i})$$
$$=-M_dc_{p,F}\frac{dT_d}{dt}-\dot{M}_d\Delta h_{lg}, \tag{19}$$

where $\mathrm{Nu}_{D,1}$ is due to single-phase (droplets in the gas) and $\mathrm{Nu}_{D,2}$ is due to phase change (film boiling) and surface convection (when the droplets are impinging on the regenerator) and the fuel droplet temperature T_d and $T_{r,i}$ is the temperature of the porous regenerator in contact with the droplets. The Nusselt number $\mathrm{Nu}_{D,2}$ is given in the Appendix in detail.

The corrected Nusselt number $\mathrm{Nu}_{D,1}$ in the convective ambient is expressed

$$\frac{\mathrm{Nu}_{D,1}}{\mathrm{Nu}_{D,1}(\mathrm{Re}_D=0)}=1+f(\mathrm{Re}_D,\mathrm{Pr}), \tag{20}$$

where $f(\mathrm{Re}_D,\mathrm{Pr})$ is the same as that given in Eq. (18), except Sc is replaced with Pr. The Nusselt number $\mathrm{Nu}_{D,1}(\mathrm{Re}_D=0)$ in the quiescent ambient.

For droplets colliding with the regenerator, the filtration efficiency is expressed as [10]

$$\alpha=\alpha_d\left[\frac{6(1-\epsilon_r)}{\pi}\right]^{1/3},\quad \alpha_d=0.093+0.387\mathrm{Sto}-0.054\mathrm{Sto}^2, \tag{21}$$

where

$$\mathrm{Sto}=\frac{\rho_{b,l}D_d^2\left|\mathbf{u}_d-\dfrac{d\mathbf{x}_r}{dt}\right|}{18\mu_f(d_s/2)},$$

where d_s is the particle diameter of porous regenerator and $\mathbf{u}_d$ is a droplet velocity.

Finally, the mass conservation equations for the gas phase, in the top and bottom gas zones, are given by

$$-(\dot{M}_{f,r})_{N_r}-\dot{M}_{F,\mathrm{evp}}=-\frac{dM_{f,t}}{dt} \tag{22}$$

$$-\dot{M}_{f,\mathrm{int}}+(\dot{M}_{f,r})_0+\dot{M}_{f,\mathrm{exh}}=-\frac{dM_{f,b}}{dt}, \tag{23}$$

where $\dot{M}_{F,\mathrm{evp}}=\sum_i^{N_d}(n_d\dot{M}_d)_i$.

The mass conservation equation for the gas phase, inside the regenerator, is given by

$$-(\dot{M}_{f,r})_{i-1}+(\dot{M}_{f,r})_i=-\frac{dM_{f,i}}{dt},\quad i=1,2,\ldots,N_r. \tag{24}$$

2.3 Regenerator Motion. The motion sequences of the piston and the bottom surface of the regenerator are given by

$$x_p=L_t-\frac{V_c}{A_{ch}}\left\{1+0.5(r_c-1)\left[1-\cos\left(\frac{\pi\theta}{180}\right)\right]\right\}, \tag{25}$$

$$x_r=a+b\theta+c\theta^2+d\theta^3+e\theta^4+f\theta^5, \tag{26}$$

where the constants a, b, c, d, e, and f are determined to satisfy the smooth transition of the velocity and the acceleration of the regenerator. Also, the minimum gaps, between the top surface of the regenerator and the cylinder head and between the bottom surface of the regenerator and the piston are needed due to the required tolerance.

The net indicated work per cycle $W_{c,\mathrm{in}}$ is given by

$$W_{c,\mathrm{in}}=\int\dot{W}_{c,\mathrm{in}}dt=\int\left[\oint\left(p_{f,t}\frac{dV_{f,t}}{dt}+p_{f,b}\frac{dV_{f,b}}{dt}\right)\right]dt. \tag{27}$$

The mechanical loss, due to the pressure drop $\Delta p=p_{f,t}-p_{f,b}$ across the porous regenerator, is expressed by

$$\dot{W}_{\mathrm{loss}}=-\oint(p_{f,t}-p_{f,b})A_{ch}\left(\frac{dx_r}{dt}-\frac{dx_p}{dt}\right). \tag{28}$$

The relevant indicators of the engine performance are the thermal efficiency η_T, the volumetric efficiency η_V, the net indicated mean-effective pressure $p_{\mathrm{mep,in}}$, the indicated specific fuel consumption sfc, and the fuel conversion efficiency η_F. The thermal efficiency η_T is defined as

$$\eta_T=\frac{W_{c,\mathrm{in}}}{-M_{r,F}\Delta h_{r,F}},\quad M_{r,F}=\int_{t_{F,s}}^{t_{F,e}}\dot{M}_{r,F}dt. \tag{29}$$

The volumetric efficiency η_V is

$$\eta_V=\frac{M_a(\theta_{v,e,i})}{M_{a,o}}, \tag{30}$$

where $M_a(\theta_{v,e,i})$ is the amount of mass of air in the cylinder when the intake valve closes and $M_{a,o}$ is the amount of air in the cylinder when charged under the inlet conditions of the intake valve.

The net indicated mean-effective pressure $p_{\mathrm{mep,in}}$, the specific fuel consumption sfc and the fuel conversion efficiency η_F are given by

$$p_{\mathrm{mep,in}}=\frac{W_{c,\mathrm{in}}}{V_d},\quad \mathrm{sfc}=\frac{M_{F,o}}{W_{c,\mathrm{in}}}\quad \eta_F=\frac{\mathrm{sfc}}{\Delta h_{r,F}}. \tag{31}$$

The energy and species conservation equations are solved with an IMSL solver (DIVPAG) capable of solving the stiff ordinary differential equations. The quasi-steady state (time periodic) solution is found when the overall energy balance error is less than 2~3 percent. The parameters used for the numerical simulation are listed in Table 2 and the operational characteristics are listed in Table 1.

Table 2 Characteristic dimensions and properties of the regenerative Diesel engine

Parameter	Magnitude	Parameter	Magnitude
cylinder:		fuel:	
D_B	0.125 m	M_F	142.3 kg/kmole
L	0.14 m	Δh_{lg}	116×10^3 J/kg-fuel
cylinder head:		$\rho_{b,l}$	853 kg/m^3
ρ_{ch}	5,200 kg/m^3	$c_{p,F}$	3,010 J/kg-K
$c_{p,ch}$	730 J/kg-K	$k_{F,v}$	54×10^{-3} W/m-K
k_{ch}	1.2 W/m-K	$\epsilon_{r,F}$	0.75
l_{ch}	2 cm	$D_{m,F}$	6×10^{-6} m^2/s
cylinder block:		T_c	617.6 K
ρ_{cb}	7,200 kg/m^3	p_c	2.096 MPa
$c_{p,cb}$	480 J/kg-K	reaction:	
k_{cb}	54 W/m-K	$\Delta h_{r,F}$	-42.5×10^6 J/kg-fuel
l_{cb}	2 cm	a_r	5.4×10^8
piston:		a_F	0.25
ρ_p	2,750 kg/m^3	a_O	1.0
$c_{p,p}$	915 J/kg-K	ΔE_a	1.256×10^8 J/kmole-K
k_p	155 W/m-K	NO formation:	
l_p	2 cm	a_r	5.74×10^{14} (cm^3/mol)$^{\frac{1}{2}}$/s
$\alpha_{r,ch/cb/p}$	0.7/0.5/0.5	ΔE_a	5.562×10^8 J/kmole-K
$\epsilon_{r,ch/cb/p}$	0.7/0.5/0.5	air:	
regenerator:		M_a	28.96 kg/kmole
ρ_r	200 kg/m^3	γ	1.4
$c_{p,r}$	1,300 J/kg-K	$c_{p,a}$	1,300 J/kg-K
k_r	63 W/m-K	gas mixture:	
$\alpha_{r,r}$	0.9	M_g	28.6 kg/kmole
$\epsilon_{r,r}$	0.9	$c_{p,f}$	1,600 J/kg-K
l_r	8 mm	k_f	0.0824 W/m-K
ϵ_r	0.7	μ_f	52.1×10^{-6} Pa-s
A_{sf}/V	11,602 m^2/m^3	Pr	1.0
d_s	150 μm	Sc	1.0
D_p	50 μm	$\alpha_{r,f}$	0.1
T_{sl}	2,700 K	$\epsilon_{r,f}$	0.1
$T_{r,max}$	1,600 K		

3 Results and Discussion

The results on engine performance, enhanced droplet evaporation, and superadiabatic combustion, and optimization of thermal regeneration are given below.

3.1 Thermal and Mechanical Performance. The $(p-V)_f$ diagram obtained from the analysis of the conventional and regenerative Diesel engines is shown in Fig. 3. The thermodynamic limit results, shown in Fig. 3, assume a constant volume process during thermal regeneration and a maximum regenerator temperature below $T_{r,\max}=1600$ K. The work gained due to thermal regeneration is denoted as A_1-A_2. Compared to the thermodynamic limit, the work loss due to insufficient thermal regeneration and the pressure drop through the regenerator (denoted as *B*), and the prolonged combustion of the Diesel engine (denoted as *C*), are detrimental to the thermal efficiency. The optimum performance should reduce the pressure drop and improve the combustion characteristics. Note that the compression ratio of the regenerative Diesel engine is lower than that of the conventional engine. This is due to the regenerator volume ($l_r=8$ mm), the gap (0.5 mm) between the regenerator top surface and the cylinder head, and the gap (1 mm) between the regenerator bottom surface and the piston.

Figure 4 shows the mass flow rate during the intake, $\dot{M}_{f,\text{int}}$, the mass flow rate during the exhaust stroke, $\dot{M}_{f,\text{exh}}$, the mass flow rate into the top gas zone from the regenerator, $(\dot{M}_{f,r})_{N_i}$, and the fuel evaporation rate, $\dot{M}_{F,\text{evp}}$. Note that the intake flow of $\dot{M}_{f,\text{int}}$ has a back flow due to the reversal of the pressure difference between the valve inlet and the bottom gas zone, and that there is a reciprocating flow of $(\dot{M}_{f,r})_{N_i}$ through the porous regenerator. The reciprocating flow is attributed to the pressure differences caused by the regenerator/piston motion, the heat transfer, and the combustion. This allows for the thermal regeneration of the flue gas heat resulting in a superadiabatic combustion.

Figure 5 shows the variations of the mass, volume, and temperatures of the top and bottom gas zones, and the top gas zone pressure during the cycle. Since thermal regenerative heating occurs after the intake valve is closed, the volumetric efficiency of the regenerative engine is not deteriorated by the thermal regeneration. The high volumetric efficiency of 92 percent is due to the surface temperature in the bottom gas zone (exposed to the intake air), which remains close to that of the conventional Diesel engine.

The temperature variations of the solid and gas phases during a cycle are shown in Fig. 6. Fuel evaporation and combustion occur during thermal regeneration resulting in a high peak gas temperature in the top gas zone and a relatively low peak gas temperature in the bottom gas zone. Note also that the ceramic cylinder head is insulated from the cylinder block (made of cast iron). The surface

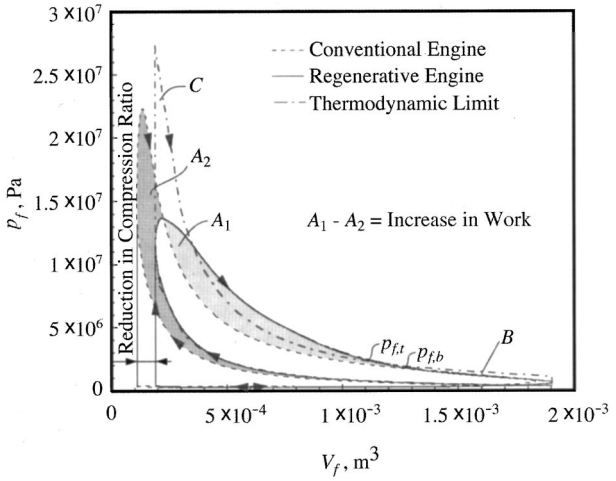

Fig. 3 Thermodynamic limit and predicted $(p-V)_f$ diagram from the start of cycle θ=0 deg to the end θ=720 deg, for the conventional and regenerative engines

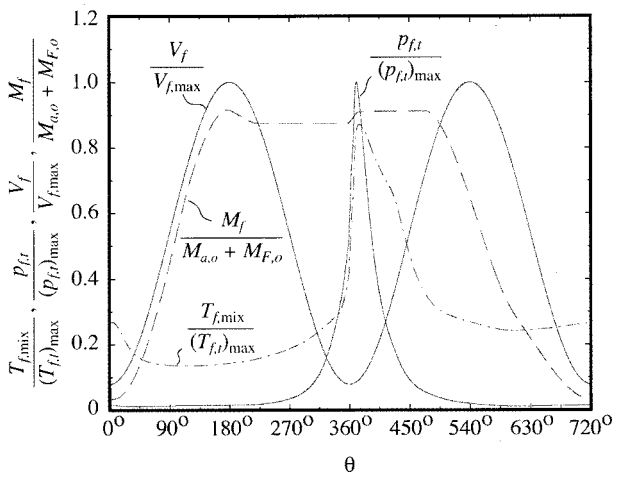

Fig. 5 Variations of dimensionless mass, volume, temperature (top and bottom gas zones), and pressure in top gas zone, during a cycle

temperature of the cylinder head $T_{ch,o}$ is higher than that of the conventional Diesel engine, but the surface temperatures of the cylinder block $T_{cb,o}$ and the surface temperature of the aluminum piston $T_{p,o}$ are lower. The surface temperature $T_{r,L}$ of the regenerator made of SiC, also has a large temperature variation.

The energy conversion, and surface heat transfer rates in the top and bottom gas zones are shown in Figs. 7(*a*) to (*c*). The heat release rate $\dot{S}_{r,c}$ is controlled only by fuel evaporation (due to the assumed perfect mixing). The heat transfer rate, Q_u, due to the thermal regeneration, shown in Figs. 7(*b*) and (*c*), enhances the fuel evaporation and leads to a superadiabatic combustion. Also the surface-radiation heat transfer $-(\dot{S}_{e,\epsilon}+\dot{S}_{e,\alpha})_t$ in the top chamber is comparable to the surface-convection heat transfer $\langle Q_{ku}\rangle_{D_B}$, due to the high surface temperature as shown in Fig. 7(*b*).

Under the baseline conditions (including $r_c=10$) given in Table 1, the predicted thermal efficiency of the regenerative engine is $\eta_T=53$ percent, the volume efficiency is $\eta_V=92$ percent, the indicated mean-effective pressure is $p_{\text{mep,in}}=2.82$ MPa, and the indicated specific fuel consumption is sfc=160 g/kW-hr.

3.2 Enhanced Evaporation. Since the fuel is injected toward the regenerator, which is located near the fuel injection nozzle, droplet impingement onto the regenerator is likely. The impinging droplets experience film boiling once in contact with the high temperature (above the Leidenfrost temperature) regenerator pore surface and are quickly vaporized. In addition to the high gas temperature (due to the thermal regeneration), the fuel impingement on the high temperature pore surface drastically reduces the evaporation time. Optimal fuel injection aims to achieve rapid fuel vaporization and uniform vapor distribution (in the top gas zone) with the least thermal impact on the porous regenerator, for the maximum performance.

The spray divergence angle θ_d is determined from the empirical correlation for a given nozzle geometry [5] and is given as

$$\tan\left(\frac{\theta_d}{2}\right)=\frac{4\pi}{4.9}\left(\frac{\rho_{f,t}}{\rho_{F,l}}\right)^{1/2}\frac{\sqrt{3}}{6}. \tag{32}$$

Figure 8(*a*) shows the penetration of the fuel spray into the top gas zone and the consequent impingement onto the moving regenerator. Figure 8(*b*) shows the fuel evaporation rate and the trajectories of the fuel droplet parcels (1st, 20th, 40th, and 50th of the 50 droplet parcels), the regenerator, and the piston. Once the fuel droplet makes contact with the porous regenerator, the fuel evapo-

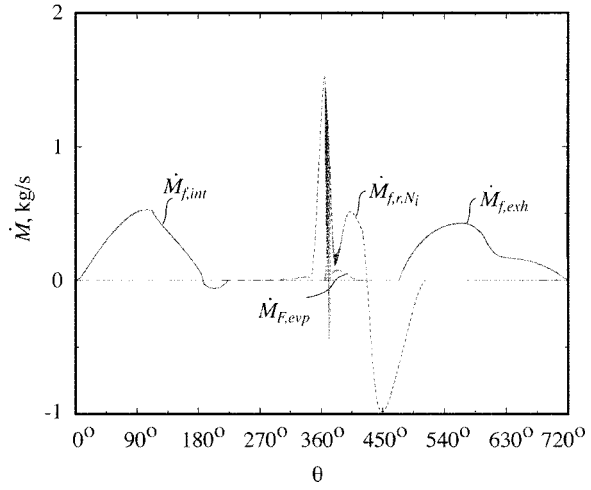

Fig. 4 Variation of mass flow rates during the intake and exhaust strokes, and the mass flow rate through the insert during the compression and expansion strokes, during a cycle

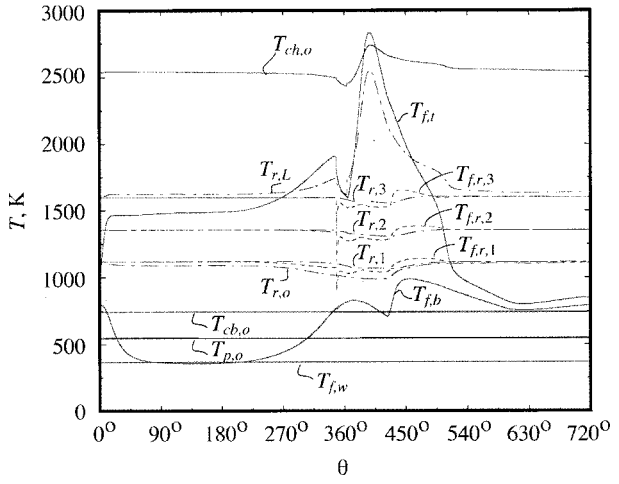

Fig. 6 Variations of the gas and solid temperatures during a cycle

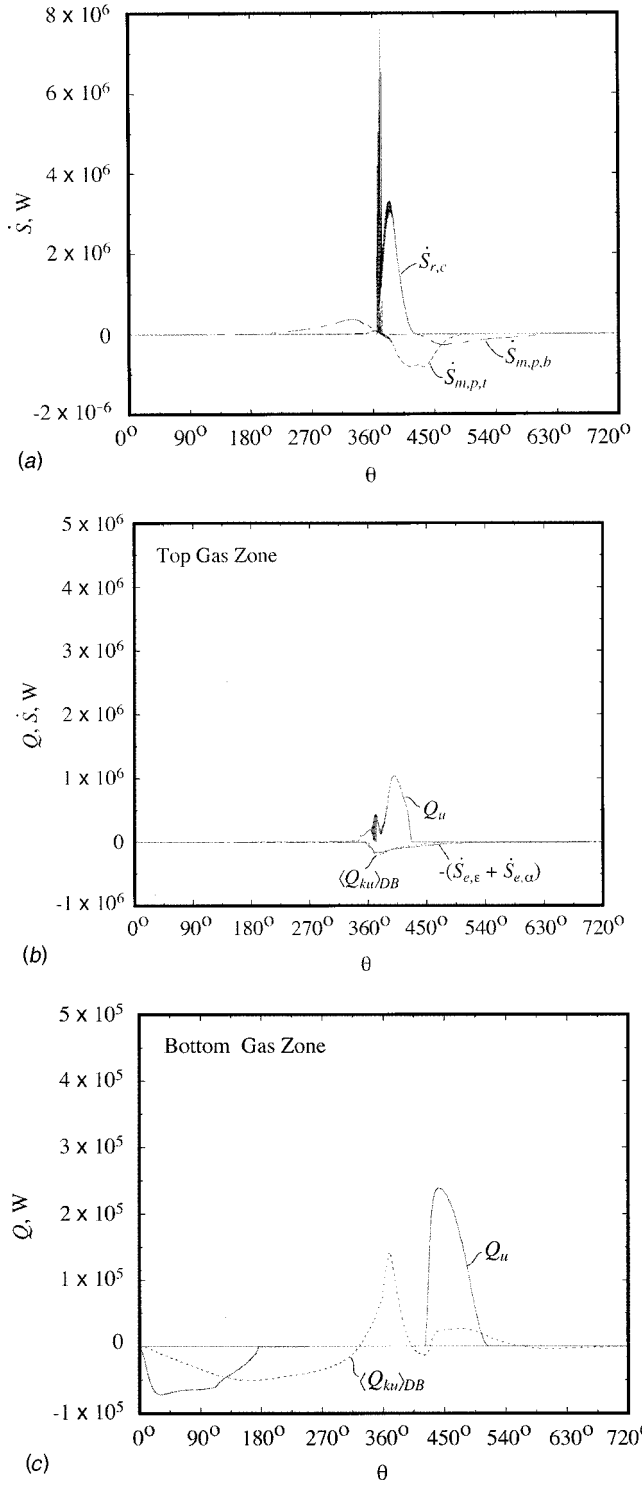

Fig. 7 Variation of the energy conversions (*a*) and heat transfer rates (*b*) and (*c*), during a cycle

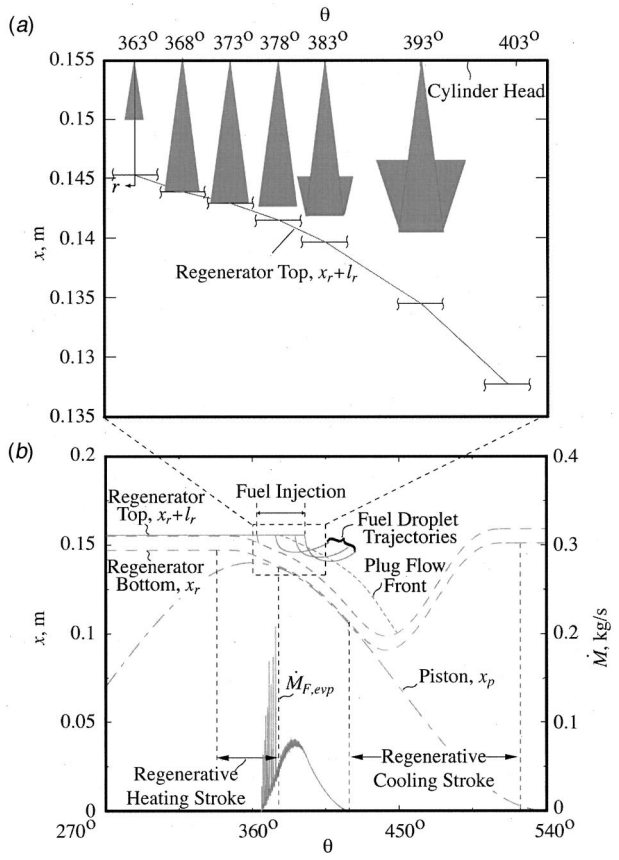

Fig. 8 (*a*) Penetration and surface impingement of fuel spray, and (*b*) the trajectories of the fuel droplets and the front location for plug gas flow in top gas zone

ration rate $\dot{M}_{F,\mathrm{evp}}$ rapidly increases. The evaporation of the captured droplets helps to provide rapid fuel evaporation enabling intense premixed combustion, and increasing the peak pressure and the thermal efficiency. The air flow emanating from the regenerator deflects the droplets and helps to provide a uniform fuel-vapor distribution in the top gas zone. Using a plug flow model for this air flow, Fig. 8(*b*) shows that the front of the plug flow reaches the cylinder head for most of the fuel injection period and, therefore, ideal perfect mixing in the top gas zone can be justifiably used.

Since the regenerator moves with a high acceleration during the thermal regeneration, excess thermal stress due to the variation of the solid temperature should be avoided. To reduce the thermal stress, surface vaporization cooling due to the impinging fuel droplets should be distributed over a larger portion of the regenerator area, thus minimizing the temperature variation along the

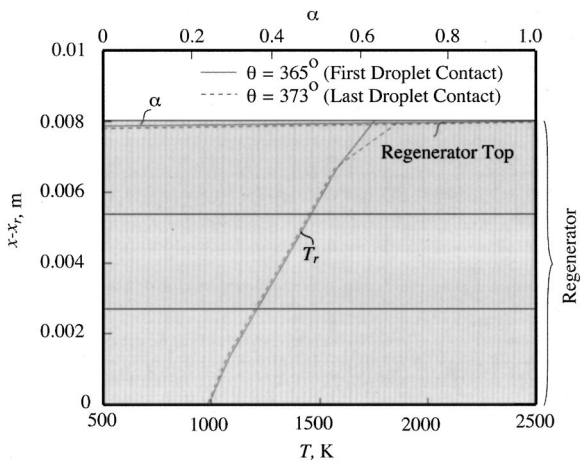

Fig. 9 The fuel droplet particle density of the first, impinging fuel droplet parcel and last parcel, and the temperature distribution within the regenerator insert

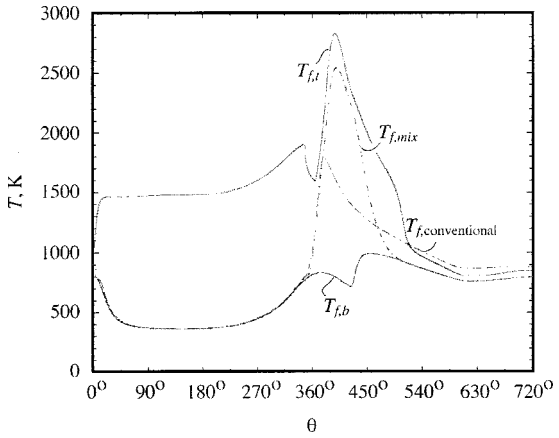

Fig. 10 Variations of gas temperatures in the regenerative and the conventional engines, during a cycle

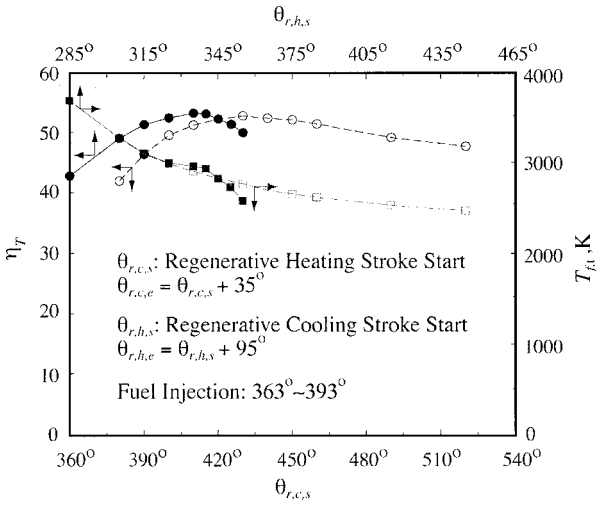

Fig. 11 Effect of the regenerative heating and cooling stroke periods on the thermal efficiency

regenerator surface. Figure 9 shows that the filtration efficiency α of the first and last impinging fuel droplet parcels captured within about 4 pores (<1 mm) for an 8 mm thickness regenerator. Also shown is that the temperature variation of the regenerator is rather small for the fuel impingement. Note that the temperature variation is affected by surface-convection, conduction, radiation, and fuel droplet evaporation.

3.3 Superadiabatic Combustion. The superadiabatic flame temperature, due to thermal regeneration of the combustion heat, increases the thermal efficiency. Figure 10 shows that the peak gas temperature $T_{f,t}$ in the top gas zone of the regenerative engine is higher than that of the conventional engine. The mixture gas temperature $T_{f,\mathrm{mix}}$ of the top and bottom gas zone is also higher than the gas temperature of the conventional engine, but only during the combustion period. The superadiabatic flame temperature during the fuel injection period enhances the fuel evaporation. The enhanced fuel evaporation assists the intense combustion resulting in an increase of the peak pressure and engine power.

The higher gas temperature, due to the superadiabatic combustion, will be beneficial in reducing the soot formation (because oxidation of the soot trapped in pores is enhanced). However, the higher gas temperature increases the thermal NO_x production. Lowering the peak flame temperature, by controlling the fuel injection timing, the thermal regeneration, and by using a fuel-lean mixture, would then become necessary to control NO_x emissions.

3.4 Optimization of Thermal Regeneration. The optimum motion schedule of the regenerator for a high thermal efficiency requires the maximum thermal regeneration and the minimum mechanical work loss due to the regenerator pressure drop.

Figure 11 shows that for the maximum thermal efficiency, the optimum regenerative heating and cooling strokes begin at 345 deg and 420 deg for prescribed stroke durations of 35 deg and 95 deg and the conditions given in Table 1, respectively (for the regenerative heating stroke, $\theta_{r,h,s} \sim \theta_{r,h,e}$, and for the regenerative cooling stroke, $\theta_{r,c,s} \sim \theta_{r,c,e}$). The optimum regenerative heating stroke would create a high gas temperature and more fuel impingement on the regenerator, and thus enhances evaporation. A retarded regenerative heating stroke decreases thermal regeneration period during the fuel injection and therefore does not achieve a higher super-adiabatic temperature.

The optimum regenerative cooling stroke using the high exhaust temperature optimizes the work gain by the thermal regeneration and the work loss by the pressure drop. An advanced regenerative cooling stroke recovers the combustion heat at a higher temperature, thus increasing the regenerator temperature and the superadiabatic flame temperatures. The retarded regenerative cooling stroke results in a higher expansion pressure due to higher exhaust gas temperature, thus increasing the work loss due to the regenerator pressure drop.

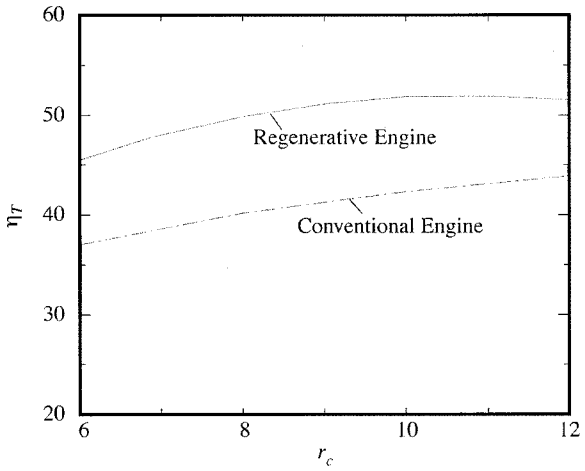

Fig. 12 Effect of compression ratio on the thermal efficiency of the regenerative and conventional engines

Figure 12 shows the effect of the compression ratio on the thermal efficiency. The maximum thermal efficiency of $\eta_T = 53$ percent is predicted at a compression ratio of $r_c = 10$. The maximum compression ratio r_c in the regenerative engine is limited to values below 14 due to the dead volume of the regenerator and the tolerance gaps. For maximum thermal efficiency, an optimum compression ratio of $r_c = 10$ is obtained.

4 Conclusion

The enhanced fuel evaporation, by droplet-regenerator interaction and air preheating, results in a more uniform fuel-vapor distribution and a dominant premixed combustion regime. The increase in the superadiabatic flame temperature enhances the fuel evaporation and increases the peak pressure, which correspondingly increases the thermal efficiency. Here the fuel-injection timing and the motion of the regenerator are optimized for a higher thermal efficiency. For the optimum compression ratio of $r_c = 10$, a thermal efficiency of $\eta_T = 53$ percent is predicted, compared to 43 percent of the conventional Diesel engine with a

Table 3 Comparison of results for conventional (non-regenerative) and regenerative Diesel engines

		Non-regenerative	Regenerative Engine
V_d	cm^3	1,718	1,718
V_c	cm^3	110.8	245.4
r_c		16.5	10
$M_{a,o}$	g	6.494	6.494
$M_{F,o}$	g	0.2165	0.2165
$(A/F)_a$		30	30
$p_{f,max}$	MPa	23.9	top: 30.3
	MPa		bottom: 30.3
$T_{f,max}$	K	1,619	top: 2,305
	K		bottom: 964
$\overline{T_{exh}}$	K	882	780
$W_{c,i,n}(720°)$	kJ	3.97	4.86
$P_{c,i}(720°)$	kW	53.0	64.8
$p_{mep,i,n}$	MPa	2.31	2.82
η_F		0.43	0.53
η_V		0.94	0.92
sfc	g/kW-hr	196	160

higher compression ratio. The performance comparison between the conventional (non-regenerative) and regenerative Diesel engines is listed in Table 3.

Acknowledgments

We are thankful to Mr. John M. Clarke at Caterpillar Inc. and Dr. Allan J. Ferrenberg at ReGen Inc. for the valuable comments on the simulation of the regenerative engine. We would also like to thank to Dr. Amir A. M. Oliveira for his start of simulation of the regenerative engine in our laboratory. The financial support of Caterpillar is greatly appreciated.

Nomenclature

a_r = frequency factor (s^{-1})
$a,b,\ldots f$ = coefficients of insert motion
A = area (m^2) or air
B_M = mass transfer number
c_p = specific heat capacity (J/kg-K)
C_D = drag coefficient
d = diameter (m)
D = diffusion coefficient (m^2/s) or diameter (m)
F = fuel
F_{i-j} = view factor
k = thermal conductivity (W/m-K)
K = permeability (m^2)
l = thickness (m)
L = length (m)
M = mass (kg) or molar weight (kg/kmole)
n = particle density per a parcel ($1/m^3$)
N = rpm (rot/min) or number of nodes or number of parcels
NTU = number of transfer units
Nu_D = Nusselt number based on D
p = pressure (Pa)
P = combustion product species
Pr = Prandtl number
q = heat flux (W/m^2)
Q = heat flow rate (W)
Q_k = conduction heat flow rate (W)
Q_{ku} = surface-convection heat flow rate (W)
Q_u = convection heat flow rate (W)
Q_r = surface radiation heat flow rate (W)
r = radial axis (m)
r_c = compression ratio
R = thermal resistance (K/W)
R_g = universal gas constant 8.3145 J/mole-K
Re_D = Reynolds number based on D
S = energy conversion rate (W)
Sc = Schmidt number
Sto = Stoke number
t = time (s)
T = temperature (K)
u = velocity (m/s)
V = volume (m^3)
W = work (J)
x = coordinate axes (m) or partial pressure

Greek

α = absorption coefficient or filtration efficiency
ΔE_a = activation energy (J/mole-K)
Δh_{lg} = heat of the phase change (J/kg)
$\Delta h_{r,F}$ = heat of reaction of fuel (J/kg-fuel)
Δl = nodal length (m)
Δp = pressure drop (Pa)
ϵ = emissivity or radiation or porosity
η_T = thermal efficiency, see Equation (25)
μ = viscosity (Pa-s)
ρ = density (kg/m^3)
θ = crank angle (degree)
σ_{SB} = Stefan-Boltzmann constant
Σ = summation
Φ = stoichiometric ratio

Subscripts

a = activation or air
A = surface or air
ad = adiabatic
b = bottom gas zone or bulk or blackbody
B = cylinder bore
c = combustion or compression or clearance or cooling
cb = cylinder block
ch = cylinder head
d = droplet or displacement or divergence
D = diameter or drag
e = exhaust or end or emission
exh = exhaust
evp = evaporation
f = fluid
F = fuel
g = gas phase
i = node index or porous insert or intake
id = ignition delay
in = indicated variable
inj = fuel injection
ins = porous insert
int = intake
k = conduction
ku = surface convection
l = liquid
loss = loss
lg = liquid-gas
n = ambient
m = mass diffusion or mass
max = maximum
mep = mean effective pressure
o = reference
O = oxidant species
p = pressure or piston or pore or plug flow
P = product species
r = radiation or reaction
R = reactant species
s = solid phase or start or particle stoichiometric
sfc = specific fuel consumption (g/kW-hr)
sl = solid-liquid

sg = saturation gas
sat = saturation
sf = solid-fluid interface
sfc = indicated specific fuel consumption
SM = Sauter mean diameter
t = top gas zone or thermal or total
T = thermal or isentropic
u = convection
v = vapor or valve
V = volume
w = cooling water
x = x-component

Other symbols

$\langle\ \rangle$ = local spatial averaged
$[\ ]$ = species concentration (mol/cm^3)

Appendix

Terms appearing in the energy conservation Eq. (2) of the top gas zone are given below. The heat transfer due to the fuel injection is

$$Q_{u,\mathrm{inj}} = -\dot{M}_{F,\mathrm{inj}} c_{p,F} T_{F,o}\,. \tag{A.1}$$

The surface-convection heat transfers between the top gas zone and surfaces of the cylinder head, the cylinder block, and the top regenerator surface $\langle Q_{ku}\rangle_{D_B}$, are

$$\langle Q_{ku,t-ch}\rangle_{D_B} = \frac{(T_{f,t}-T_{ch,o})}{\langle R_{ku,t-ch}\rangle_{D_B}}, \quad \langle Q_{ku,t-cb}\rangle_{D_B} = \frac{(T_{f,t}-T_{cb,o})}{\langle R_{ku,t-cb}\rangle_{D_B}},$$

$$\langle Q_{ku,t-r}\rangle_{D_B} = \frac{(T_{f,t}-T_{r,L})}{\langle R_{ku,t-r}\rangle_{D_B}}, \tag{A.2}$$

where the surface-convection resistance is given as

$$\langle R_{ku,t}\rangle_{D_B} = \frac{D_B}{\langle \mathrm{Nu}\rangle_{D_B,t} k_f A_{ku,t}}, \tag{A.3}$$

where $\langle \mathrm{Nu}\rangle_{D_B,t}$ is determined from the Woschni correlation using the average cylinder gas velocity and the cylinder pressure [11], as given below

$$\langle \mathrm{Nu}\rangle_{D_B,t} = 0.035\,\mathrm{Re}_{D_B,t}^{0.8}, \quad \mathrm{Re}_{D_B,t} = \frac{\rho_{f,t} D_B \langle u_f\rangle_t}{\mu_f}. \tag{A.4}$$

Here $\langle u_f\rangle_t$ is given by

$$\langle u_f\rangle_t = c_1 (\overline{u_{p,t}^2})^{1/2} + c_2 \frac{V_f (p_{f,t}-p_m)}{(M_{a,o}+M_{F,o})\dfrac{R_g}{M_g}}, \tag{A.5}$$

where

$$(\overline{u_{p,t}^2})^{1/2} = 2 L_d N \frac{2\pi(\mathrm{rad/rot})}{60(\mathrm{s/min})}, \quad p_m V_f = M_f \frac{R_g}{M_g} T_n \tag{A.6}$$

and $c_1 = 0.57$, $c_2 = 0$ m/s-K, and for only expansion, $c_1 = 0.57$, $c_2 = 0.00081$ m/s-K. Note that c_1 and c_2 are determined by the calibration of current simulation results against the Caterpillar's engine simulation code which has similar submodels to the current simulation code.

The energy conversion terms in the top gas zone are

$$\dot{S}_{r,c} = \dot{M}_{r,F} \Delta h_{r,F}, \quad \dot{S}_{m,p,t} = V_{f,t} \frac{dp_{f,t}}{dt}, \quad \dot{S}_{F,lg} = -\dot{M}_{F,\mathrm{evp}} \Delta h_{lg},$$

$$\begin{aligned}(\dot{S}_{e,\epsilon} + \dot{S}_{e,\alpha})_t = {} & (-\epsilon_{r,f}\alpha_{r,ch}\sigma_{\mathrm{SB}} T_{r,f,t}^4 + \epsilon_{r,ch}\alpha_{r,f}\sigma_{\mathrm{SB}} T_{ch,o}^4) A_{r,ch} \\ & + (-\epsilon_{r,f}\alpha_{r,cb}\sigma_{\mathrm{SB}} T_{r,f,t}^4 + \epsilon_{r,cb}\alpha_{r,f}\sigma_{\mathrm{SB}} T_{cb,o}^4) A_{r,cb,t} \\ & + (-\epsilon_{r,f}\alpha_{r,r}\sigma_{\mathrm{SB}} T_{r,f,t}^4 + \epsilon_{r,r}\alpha_{r,f}\sigma_{\mathrm{SB}} T_{r,L}^4) A_{r,r}\,.\end{aligned} \tag{A.7}$$

Note that the $T_{r,f,t}$ is the apparent flame temperature for the gas volumetric radiation [12] and the $T_{r,L}$ is the top surface temperature of the regenerator.

For the bottom gas zone, the convection heat transfer due to gas flow through the regenerator, the intake and the exhaust are

$$Q_{u,\mathrm{int}} = \begin{cases} -\dot{M}_{a,\mathrm{int}} c_{p,f} T_n & \text{for } \dot{M}_{a,\mathrm{int}} \geqslant 0 \\ \dot{M}_{a,\mathrm{int}} c_{p,f} T_{f,b} & \text{for } \dot{M}_{a,\mathrm{int}} < 0 \end{cases}$$

$$Q_{u,\mathrm{exh}} = \begin{cases} -\dot{M}_{a,\mathrm{exh}} c_{p,f} T_{f,b} & \text{for } \dot{M}_{a,\mathrm{exh}} \geqslant 0 \\ \dot{M}_{a,\mathrm{exh}} c_{p,f} T_e & \text{for } \dot{M}_{a,\mathrm{exh}} < 0\,. \end{cases} \tag{A.8}$$

Note that the intake and exhaust occurs in the bottom chamber. The surface-convection heat transfers $\langle Q_{ku,b-cb}\rangle_{D_B}$, $\langle Q_{ku,b-p}\rangle_{D_B}$, $\langle Q_{ku,b-r}\rangle_{D_B}$ are determined similarly as in the top chamber.

In the regenerator, the conduction heat transfer rate in the solid phase is given by

$$(Q_{k,r})_{i-(i+1)} = \frac{T_{r,i}-T_{r,i+1}}{(R_{k,r})_{i-(i+1)}}, \quad (R_{k,r})_{i-(i+1)} = \frac{\Delta l_{r,i}}{(1-\epsilon_r) A_r k_r}. \tag{A.9}$$

The surface-convection heat transfer between the porous regenerator and the gas is given by

$$\langle Q_{ku,f-r}\rangle_i = \frac{\langle \mathrm{Nu}\rangle_{D,p,i} k_f}{D_p} \frac{A_{sf}}{V} (\Delta l_{r,i} A_r)(T_{r,i} - T_{f,r,i}) \tag{A.10}$$

where

$$\langle \mathrm{Nu}\rangle_{D,p,i} = 2 + (0.4\,\mathrm{Re}_{D,p,i}^{1/2} + 0.2\,\mathrm{Re}_{D,p,i}^{2/3})\mathrm{Pr}^{0.4}$$

$$\mathrm{Re}_{D,p,i} = \frac{\dot{M}_{f,r,i} D_p}{(1-\epsilon_r) A_r \mu_f}, \quad D_p = 6(1-\epsilon_r)\frac{V}{A_{sf}}.$$

It is assumed that the heat transfer due to the fuel droplet-regenerator interaction occurs between the fuel droplet and the solid phase of the regenerator. The heat transfer due to the fuel droplet in contact with the regenerator is given by

$$Q_{d,i} = n_d \alpha_d \frac{\mathrm{Nu}_{D,2} k_f}{D_d} A_d (T_d - T_{r,i}), \tag{A.11}$$

where $\mathrm{Nu}_{D,2}$ is due to the film boiling heat transfer for the droplets colliding the porous regenerator over Leidenfrost temperature and is expressed as [13]

$$\begin{aligned}\mathrm{Nu}_{D,2} = \frac{D_d}{k_f}\Bigg[& \rho_{b,l}\Delta h_{lg,\infty} \frac{\langle \dot{m}_d\rangle}{\rho_{b,l}} \eta_d \left\{ 1 - \frac{\langle \dot{m}_d\rangle/\rho_{b,l}}{(\langle \dot{m}_d\rangle/\rho_l)_o} \right\} \frac{1}{T_{r,i}-T_d} \\ & + 1720 (T_{r,i}-T_d)^{-0.088} D_d^{-1.004} u_d^{-0.764} \frac{(\langle \dot{m}_d\rangle/\rho_{b,l})^2}{(\langle \dot{m}_d\rangle/\rho_l)_o} \Bigg],\end{aligned} \tag{A.12}$$

where

$$\eta_d \equiv \frac{3.68\times 10^4}{\rho_{b,l}\Delta h_{lg,\infty}} (T_{r,i}-T_d)^{1.691} D_d^{-0.062}$$

$$\Delta h_{lg,\infty} \equiv c_{p,l}(T_{lg}-T_d) + \Delta h_{lg}$$

$$\left(\frac{\langle \dot{m}_d\rangle}{\rho_l}\right)_o \equiv 5\times 10^{-3}\ \text{m/s}.$$

Note that the above correlation is based on experimental results for water droplet spray on a nickel-plated copper surface, in an otherwise stagnant air is used for $180°\mathrm{C} < T_{r,i} - T_{l,\infty} < 380°\mathrm{C}$. Although the regenerator surface condition is out of the range considered, it is assumed that the relation can be used for the analysis of the impinging droplets in the vapor-film regime.

In the regenerator, the convection heat transfer rate for the fluid phase is given by

$$(Q_{u,r})_i=\begin{cases}(\dot{M}_{f,r})_i c_{p,f} T_{f,r,i} & \text{for } (\dot{M}_{f,r})_i \geqslant 0\\ -(\dot{M}_{f,r})_i c_{p,f} T_{f,r,i+1} & \text{for } (\dot{M}_{f,r})_i < 0.\end{cases}$$
$$i=0,1,\ldots,N_r, \qquad (A.13)$$

where $T_{f,r,0}=T_{f,b}$ and $T_{f,r,N_r+1}=T_{f,t}$.

At the bottom surface of the porous regenerator $i=1$, the energy equation is

$$-\frac{(T_{f,b}-T_{r,o})}{\langle R_{ku,b-r}\rangle_{D_B}}+\frac{T_{r,o}-T_{r,1}}{(R_{k,r})_{o-1}}=0. \qquad (A.14)$$

At the top surface of the porous regenerator $i=N_r$, the energy equation is

$$-\frac{(T_{f,t}-T_{r,L})}{\langle R_{ku,t-r}\rangle_{D_B}}-\frac{\sigma_{SB}(T_{cb,o}^4-T_{r,L}^4)}{(R_{r,\Sigma})_{cb-r,t}}-\frac{T_{r,N_r}-T_{r,L}}{(R_{k,r})_{N_r-L}}$$
$$=-\dot{S}_{e,\epsilon,r}-\dot{S}_{e,\alpha,r}, \qquad (A.15)$$

where $(R_{r,\Sigma})_{cb-r,t}$ is the surface radiation resistance [14]

$$(R_{r,\Sigma})_{cb-r,t}=\frac{1-\epsilon_{r,cb}}{\epsilon_{r,cb}A_{r,cb}}+\frac{1}{F_{cb-r}(A_{r,cb})_t}+\frac{1-\epsilon_{r,r}}{\epsilon_{r,r}A_{r,r}}.$$

Note that the surface and volumetric radiation are neglected at the bottom chamber due to the low temperature.

In the energy conservation equation for the cylinder head, the heat transfer rates are given by $(Q|_{A,ch})_i$ is given for the volumes $i=1,2,\ldots N_{ch}-1$ as

$$(Q|_{A,ch})_i=-\frac{(T_{ch,i-1}-T_{ch,i})}{(R_{k,ch})_{(i-1)-i}}+\frac{(T_{ch,i}-T_{ch,i+1})}{(R_{k,ch})_{i-(i+1)}}, \qquad (A.16)$$

and for the inside surface of cylinder head, the energy equation is given by

$$-\frac{(T_{f,t}-T_{ch,o})}{\langle R_{ku,t-ch}\rangle_{D_B}}+\frac{\sigma_{SB}(T_{ch,o}^4-T_{r,L}^4)}{(R_{r,\Sigma})_{ch-r,t}}+\frac{\sigma_{SB}(T_{ch,o}^4-T_{cb,o}^4)}{(R_{r,\Sigma})_{ch-cb,t}}$$
$$+\frac{(T_{ch,o}-T_{ch,1})}{(R_{k,ch})_{o-1}}=-\dot{S}_{e,\epsilon,ch}-\dot{S}_{e,\alpha,ch}, \qquad (A.17)$$

and for the last volume $i=N_{ch}$, we have

$$(Q|_{A,ch})_{N_{ch}}=-\frac{(T_{ch,N_{ch}-1}-T_{ch,N_{ch}})}{(R_{k,ch})_{(N_{ch}-1)-N_{ch}}}+\frac{(T_{ch,N_{ch}}-T_{f,w})}{R_{k,ch-w}+(R_{ku,f})_w}, \qquad (A.18)$$

where $(R_{ku,f})_w$ is the thermal resistance for surface convection in the coolant jacket.

For the mass conservation equation, the fuel evaporation rate $\dot{M}_d(\mathrm{Re}_D=0)$ in the quiescent ambient is [9]

$$\dot{M}_d(\mathrm{Re}_D=0)=2\pi\rho_{f,t}D_d D_{m,F}\ln(1+B_M), \qquad (A.19)$$

where

$$B_M=\frac{Y_{F,sg}-Y_{F,\infty}}{1-Y_{F,sg}}.$$

The saturation fuel-vapor concentration $Y_{F,sg}$ is determined as

$$Y_{F,sg}=\frac{x_{sg}M_F}{(1-x_{sg})M_a+x_{sg}M_F}, \qquad (A.20)$$

where

$$x_{sg}=\frac{p_v}{p_{f,t}}, \quad p_v=p_{v,o}e^{(-M_v\Delta h_{lg}/R_g)(1/T_d-1/T_{lg,o})}.$$

From the mass conservation equation, the droplet diameter is given by

$$\frac{dD_d}{dt}=-\frac{4\rho_{f,t}D_{m,F}}{\rho_{b,l}D_d}\ln(1+B_M)[1+f(\mathrm{Re}_D,\mathrm{Sc})], \qquad (A.21)$$

where $D_{m,F}$ is the diffusion coefficient, D_d is the droplet diameter, and B_M are the mass transfer number.

For the energy conservation equation of the fuel droplet, Nusselt number $\mathrm{Nu}_{D,1}$ $(\mathrm{Re}_D=0)$ in the quiescent ambient is expressed

$$\mathrm{Nu}_{D,1}(\mathrm{Re}_D=0)=\frac{\dfrac{\dot{M}_d(\mathrm{Re}_D=0)c_{p,F}}{\pi D_d k_f}}{\exp\left(\dfrac{\dot{M}_d(\mathrm{Re}_D=0)c_{p,F}}{2\pi D_d k_f}\right)-1}. \qquad (A.22)$$

Species conservation equations in the top chamber are given by

$$-\dot{M}_{F,\mathrm{evp}}+\dot{M}_{r,F}=-\frac{dM_{F,t}}{dt} \qquad (A.23)$$

$$[-(\dot{M}_{f,r})_{N_r}+\dot{M}_{r,F}(A/F)_s]\left(\frac{O}{A}\right)-\frac{1}{2}\dot{M}_{NO,t}=-\frac{dM_{O,t}}{dt} \qquad (A.24)$$

$$-(\dot{M}_{f,r})_{N_r}\left[1-\left(\frac{O}{A}\right)\right]-\frac{1}{2}\dot{M}_{NO,t}=-\frac{dM_{N_2,t}}{dt}, \qquad (A.25)$$

where $M_{f,t}=M_{F,t}+M_{O,t}+M_{P,t}+M_{N_2,t}$ and $(A/F)_s=15.5$, $(O/A)_s=0.23$.

The mass of fuel injected $M_{F,o}$ is calculated as a function of the air to fuel ratio $(A/F)_a$ and the intake conditions by

$$M_{F,o}=\frac{M_{a,o}}{(A/F)_a}, \quad M_{a,o}=\frac{p_n V_d}{T_n\dfrac{R_g}{M_a}}. \qquad (A.26)$$

References

[1] Ferrenberg, A. J., 1988, "Regenerative Internal Combustion Engine," US Patent 4,790,284.

[2] Ferrenberg, A. J., 1990, "The Single Cylinder Regenerated Internal Combustion Engine," SAE Paper No. 900911.

[3] Ferrenberg, A. J., Williams B. E., and McNeal, S. R., 1995, "Low Heat Rejection Regenerated Diesel Engines for Shipboard Mechanical and Electrical Power (Part2)," Contract N00167-92-C-0020.

[4] Park, C.-W., and Kaviany, M., 2000, "Combustion-Thermoelectric Tube," ASME J. Heat Transfer , **122**, pp. 721–729.

[5] Heywood, J. B., 1988, *Internal Combustion Engine Fundamentals*, McGraw-Hill.

[6] Kaviany, M., 1999, *Principles of Heat Transfer in Porous Media*, Corrected Second Edition, Springer-Verlag, New York.

[7] Westbrook, C. K., and Dryer, F. L., 1984, "Chemical Kinetic Modeling of Hydrocarbon Combustion," Prog. Energy Combust. Sci., **10**, pp. 1–57.

[8] Hiroyasu, H., and Kadota, T., 1974, "Fuel Droplet Size Distribution in Diesel Combustion Chamber," SAE Paper No. 740715.

[9] Faeth, G. M., 1983, "Evaporation and Combustion of Sprays," Prog. Energy Combust. Sci., **9**, pp. 1–76.

[10] Martynenko, V. V., Echigo, R., and Yoshida, H., 1998, "Mathematical Model of Self-Sustaining Combustion in Inert Porous Medium With Phase Change Under Complex Heat Transfer," Int. J. Heat Mass Transf., **41**, No. 1, pp. 117–126.

[11] Woshni, G., 1967, "Universally Applicable Equation for the Instantaneous Heat Transfer Coefficient in the Internal Combustion Engine," SAE Paper No. 670931.

[12] Assanis, D. N., and Heywood, J. B., 1986, "Development and Use of Computer Simulation of the Turbocompounded Diesel System for Engine Performance and Components Heat Transfer Studies," SAE Paper No. 860329.

[13] Bernardin, J. D., and Mudawar, I., 1997, "Film Boiling Heat Transfer of Droplet Streams and Sprays," Int. J. Heat Mass Transf., **40**, pp. 2579–2593.

[14] Siegel, R., and Howell, J. R., 1992, *Thermal Radiation Heat Transfer*, Third Edition, Hemisphere, Washington, D.C.